Hindawi
Applied Bionics and Biomechanics
Volume 2023, Article ID 1434832, 7 pages
https://doi.org/10.1155/2023/1434832

Research Article

Non-Newtonian Effects of Blood Flow on Hemodynamics in Pulmonary Stenosis: Numerical Simulation

Fan He,[1] **Xinyu Wang**,[1] **Lu Hua**,[2] **and Tingting Guo**[2]

[1]*School of Science, Beijing University of Civil Engineering and Architecture, Beijing 100044, China*
[2]*Thrombosis Center, National Clinical Research Center for Cardiovascular Diseases, State Key Laboratory of Cardiovascular Disease, Fuwai Hospital, National Center for Cardiovascular Diseases, Chinese Academy of Medical Sciences and Peking Union Medical College, Beijing 100037, China*

Correspondence should be addressed to Fan He; hefan@bucea.edu.cn and Lu Hua; ethannan@126.com

Received 10 September 2022; Revised 8 December 2022; Accepted 15 December 2022; Published 7 February 2023

Academic Editor: Mohammad Rahimi-Gorji

This paper aims to explore the construction of an individualized pulmonary artery stenosis model based on computed tomography (CT) images. The stenosis model is simulated using a porous medium, and the numerical simulation is carried out by computational fluid dynamics (CFD) method to discuss non-Newtonian effects on hemodynamics. The hemodynamic parameters and quantitative pulmonary pressure ratio (QPPR) of the right pulmonary artery stenosis are obtained. The change curves of hemodynamic parameters show that the effects of non-Newtonian fluid are more significant than those of Newtonian fluid. Under the non-Newtonian condition, pressure and velocity drop more and faster when blood flow enters into the stenosis region. There is a high wall shear stress in the stenosis downstream. The margin of error between the QPPR value of the non-Newtonian fluid simulation and the clinical measurement value is not more than 10%. This work provides the evidence that the simulation of non-Newtonian fluid is closer to the reality when a porous medium model is used in a stenosis model. This contributes to assessing the severity of pulmonary stenosis behavior and is essential to guide disease treatment.

1. Introduction

Chronic thromboembolic pulmonary hypertension is a long-term result of in situ pulmonary artery thrombosis or acute pulmonary embolism. Many reasons lead to thrombolysis, which has been existing through organization and fibrosis [1, 2]. Insoluble substances such as thrombus accumulate on the surface of the blood vessel wall, causing blockage of pulmonary artery branches. In clinical practice, the general diagnosis and treatment method are to evaluate the degree of blockage through pulmonary angiography observation and pulmonary vascular classification, which are divided into four levels: 0–3. The lower the level, the worse the pulmonary artery blood flow imaging, and the more serious the degree of blockage, and then different treatment methods are used [3]. In the previous simulation of arterial stenosis, most of the stenosis models ignored the internal structure of the stenosis [4, 5]. However, the angiographic characteristics of pulmonary artery occlusion can be divided into five types, including reticular and banded lesions, sudden narrowing lesions, complete occlusion lesions, cystic lesions, and intimal irregularities. Therefore, the internal structure model of the stenosis is worth studying. With the continuous combination and development of medical images and computers, noninvasive simulations of fractional flow reserve (FFR) of coronary artery have been prevalent [6–9]. In this paper, quantitative pulmonary pressure ratio (QPPR) is introduced, which is similar to FFR. It is defined as the ratio of the maximum systolic pressure at the distal end to the proximal end of stenosis. At present, clinical diagnosis of pulmonary hypertension and other diseases is mainly through the insertion of pressure guide wire from femoral vein/carotid artery, multiple perfusions of contrast agent, and to capture physiological information such as the location, degree, and morphology of stenosis [10]. Similar to the coronary FFR, this diagnostic method is invasive, expensive, and had a long diagnostic cycle for patients. It is easy to miss the best treatment time and is not conducive to the improvement of prognosis [11].

Previous studies on the hemodynamics of pulmonary artery in zero-/one-dimensional, three-dimensional (3D), and multiscale models used computational fluid dynamics (CFD) to understand the pulmonary blood flow environment, wall deformation, and other conditions. Under the conditions of stability and blood flow, researchers established three different geometric models of the human pulmonary vascular system to conduct the coupling simulation of blood flow and drug particles [12–15]. A lot of work claimed that the blood flow problem had dual behavior, namely, Newtonian and non-Newtonian. Under different fluid models, the effects of vessel wall elasticity, fluid flow and heat transfer, and blood pulsation on particle transport and deposition were studied [16–19]. As well known, blood is composed of blood cells and plasma, which is usually approximate to Newtonian fluid. However, under some conditions, such as stenosis vessels, the non-Newtonian characteristics of blood should be considered [20]. Therefore, this work discusses the differences between the two fluid models.

According to the clinical anatomy, most of the pulmonary artery blockages are like "lotus root" or "honeycomb." In this work, a porous medium model is used to simulate the stenosis, taking the solid as the skeleton, filling the pores, and using the porosity to adjust the degree of blockage. The 3D model of pulmonary artery is constructed according to the computed tomography (CT) images of a patient, and the stenotic branches and their surrounding branches are constructed. The hemodynamics and QPPR are numerically simulated by using the method of CFD, in order to study the effects of Newtonian and non-Newtonian fluids on their blood flow characteristics and to compare the hemodynamic changes under the two models.

2. Materials and Methods

2.1. Case Selection. The information collection and data source of pulmonary artery CT images are from a 50-year-old female patient in Fuwai Hospital, Chinese Academy of Medical Sciences. She suffers from chronic thromboembolic pulmonary hypertension. By placing the Terumo 5F pigtail catheter on the right pulmonary arteriography, it is found that the anterior basal segment of the right lower pulmonary artery and the outer basal end of pulmonary artery are stenosed and occluded, and the pulmonary venous reflux is significantly slowed down.

2.2. 3D Reconstruction of Vascular Model. The region of interest is obtained through image segmentation, surface smoothing, and other operations to generate a 3D pulmonary artery model. In order to ensure the feasibility of numerical calculation, the obtained 3D model is edited, and is finally imported into numerical simulation. The model is divided into wall, fluid, and porous media regions, with a wall thickness of 0.8 mm, as shown in Figure 1.

In the simulation, the model is identified and analyzed. The inlet and outlet planes are fixed. We set the grid properties (grid division method and size) and reduce the grid size in order to improve the calculation accuracy of stenosis region. After the grid independence test, the number of solid

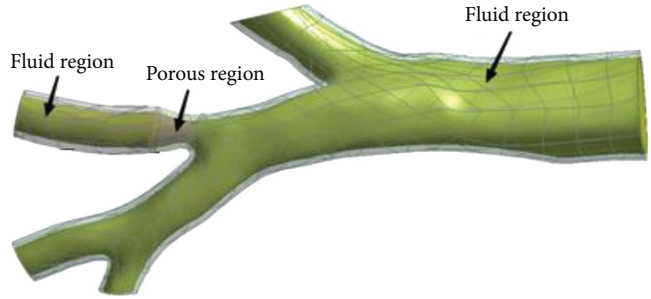

Figure 1: Pulmonary artery stenosis model.

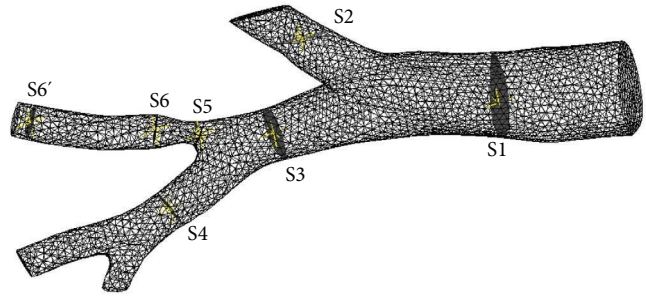

Figure 2: Sectional view of pulmonary artery stenosis.

grids is 24,223, the number of nodes is 48,146, the number of fluid domain grids is 43,667, and the number of nodes is 9,190. Seven sections are intercepted on the model for hemodynamic analysis. These sections are located in each branch of the model to facilitate the next step of analysis and processing, as shown in Figure 2.

2.3. Numerical Simulation. Blood is modeled to be non-Newtonian and Newtonian fluids, respectively. The flow is incompressible and turbulent. The Carreau–Yasuda model is used when the non-Newtonian behavior of blood is considered, and the formula is as follows:

$$\mu = \mu_\infty + (\mu_0 - \mu_\infty)[1 + (\lambda\gamma)^2]^{(n-1)/2}, \tag{1}$$

where μ is dynamic viscosity, λ is a time constant, γ is the shear rate, n is the power law exponent, $\mu_0 = 0.0560$ Pa·s, $\mu_\infty = 0.00345$ Pa·s, $\lambda = 3.313$ s, and $n = 0.3568$ [21]. When it embodies Newtonian fluid behavior, $\mu = 0.004$ Pa·s [22]. The governing equations are Navier–Stokes and continuous equations.

$$\frac{\partial u}{\partial t} + ((u - u_m) \cdot \nabla)u = -\frac{1}{\rho_f}\nabla p_d + \nabla \cdot (\nu(\nabla u + (\nabla u)^T)). \tag{2}$$

$$\nabla \cdot u = 0, \tag{3}$$

where u is the fluid velocity, u_m is the mesh velocity of the fluid, p_d is the fluid flow pressure, $\rho_f = 1{,}060$ kg/m^3 [23], and ν represents the kinematic viscosity coefficient, $\nu = (\mu)/(\rho_f)$.

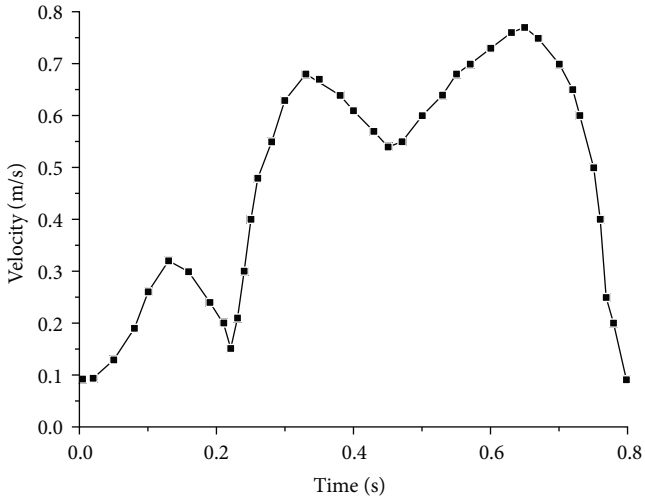

FIGURE 3: The inlet velocity.

The arterial wall is assumed to be isotropic, incompressible, and linear elastic. The governing equation is as follows [24]:

$$\rho_s a_s = \nabla \cdot \sigma_s, \tag{4}$$

where the density $\rho_s = 1{,}120\,\text{kg/m}^3$ [25], a_s represents the acceleration of the particle on the vessel wall, and σ_s represents the stress tensor of the blood vessel wall, with elastic modulus $E = 5$ MPa [24] and Poisson's ratio $\nu = 0.499$ [17]. It is worth noting that in the porous media domain, the wall is set to be rigid with a porosity of 0.5 [26].

The important feature of fluid–solid coupling is the interaction between fluid and solid structure. That is, the deformation of vessel wall under the action of blood flow is caused, and then it further affects blood flow [27]. On the interface of fluid–solid coupling, it is assumed that the motions of the fluid and wall are the same and there is no sliding.

$$\begin{aligned} u &= U, \\ L_s &= L_f, \\ \sigma_s \cdot n_s &= \sigma_f \cdot n_f, \end{aligned} \tag{5}$$

where the velocity of the solid boundary is U, σ_f is the fluid stress tensor, L_s and L_f represent the displacements of solid and fluid, respectively, and n_s and n_f are the solid and the fluid boundary normal unit vectors, respectively.

The inlet velocity is shown in Figure 3, which shows the blood flow velocity in a cardiac cycle, and the outlets are set to be 2,267 Pa (about 17 mm Hg). The initial conditions of the whole flow field are 0. The total calculation time is 2.4 s, and the period is 0.8 s. In the process of this study, the sensitivity analysis of the time step is carried out. The time step is set to 0.01 s, and the third cycle can reach the periodic stable state. The results of the third cycle are selected for the next analysis. The fluid and porous media regions are connected through the interface to ensure the continuity of mass and pressure and the conservation of mass and momentum.

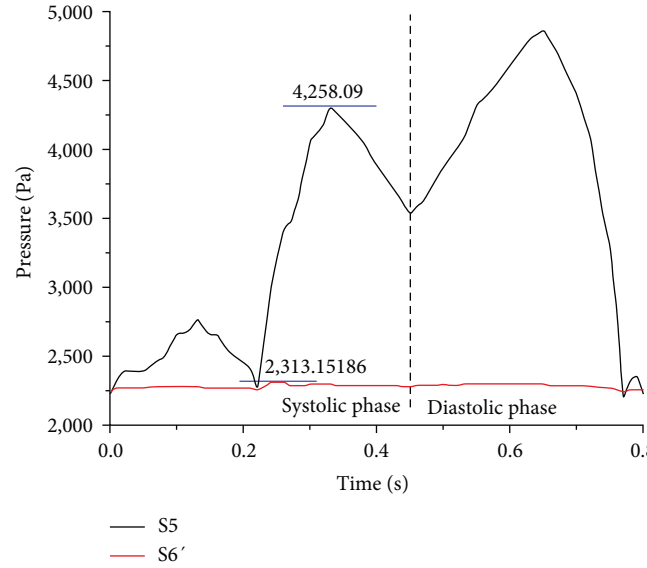

FIGURE 4: Pressures at both ends of the stenosis with the Newtonian fluid model.

3. Results

3.1. Quantitative Pulmonary Pressure Ratio. The calculation formula of QPPR in this paper is as follows:

$$\text{QPPR} = \frac{P_d}{P_a}, \tag{6}$$

where P_d and P_a, respectively, represent the maximum systolic pressure at the distal and proximal ends of the diseased vessel. The clinical measurement value of QPPR of this patient is 0.41.

The pressures at both ends of the stenosis are obtained through numerical simulation. Figure 4 describes the pressures at both ends of the stenosis with the Newtonian fluid model. During systole, the pressures at the distal and proximal ends are 2,313.15 and 4,258.09 Pa, respectively. Figure 5 shows the pressures at both ends of the stenosis with the non-Newtonian fluid model. During systole, the pressures at the distal and proximal ends are 2,327.21 and 5,328.99 Pa, respectively. It can be seen from the results that the distal pressure of the stenosis with the non-Newtonian fluid model is much higher than that with the Newtonian fluid model, but the pressure change trend is similar with the two models.

According to Equation (6), the results are obtained, as shown in Table 1. Compared with the actual measured value of 0.41, the margin of error between the measured and simulated values with the non-Newtonian fluid model is within 10%. It is concluded that the simulation effect of non-Newtonian fluid is better than that of Newtonian fluid.

3.2. Maximum Pressures. Figure 6 shows the pressure change curves of four sections (S1, S2, S3, S4) on the branches of normal artery. Whether Newtonian fluid or non-Newtonian fluid, the pressure distribution curves of all sections are similar. The pressure peak of section S1 (non-Newtonian) is the

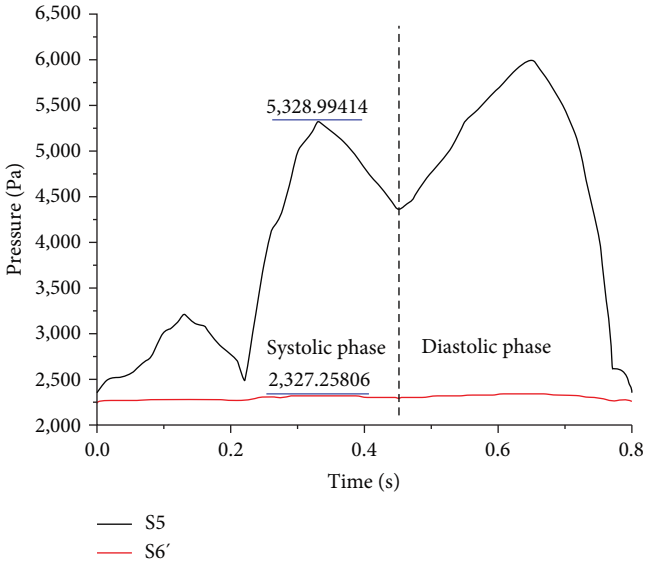

Figure 5: Pressures at both ends of the stenosis with the non-Newtonian fluid model.

Table 1: QPPR with different fluid models.

	Newtonian fluid	Non-Newtonian fluid
QPPR	0.5432	0.4367

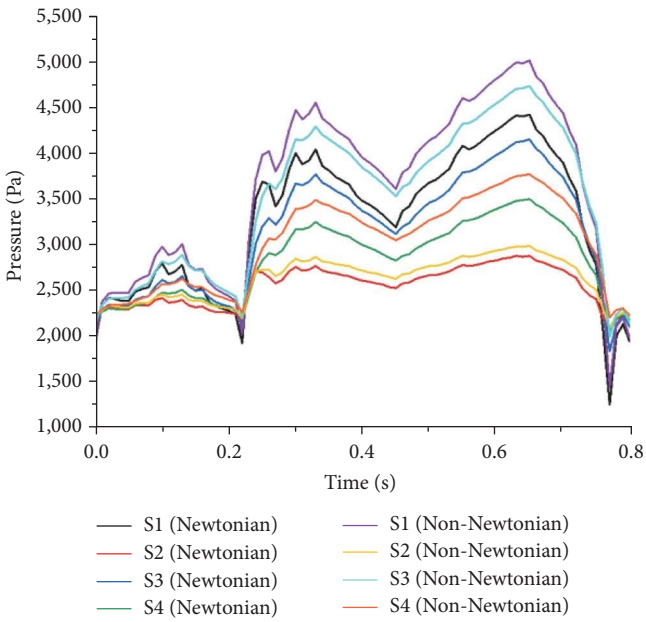

Figure 6: Maximum pressures on normal branches.

highest during two periods (systolic and diastolic), both exceeding 4,500 Pa. The pressure value of section S1 (Newtonian) is lower than 4,500 Pa. The peak pressures of section S2 (Newtonian and non-Newtonian) are about 2,600 Pa. Compared with section S4 (whether Newtonian or non-Newtonian), section S3 (whether Newtonian or non-Newtonian) has a higher pressure value. It is found

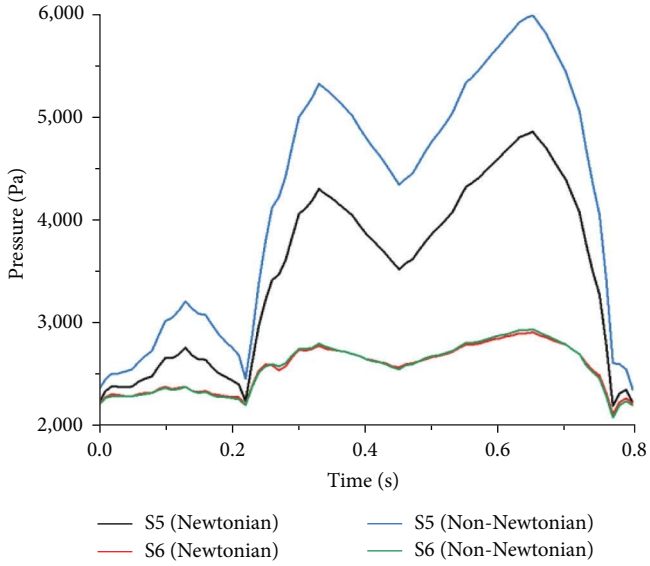

Figure 7: Maximum pressures at both ends of the stenosis.

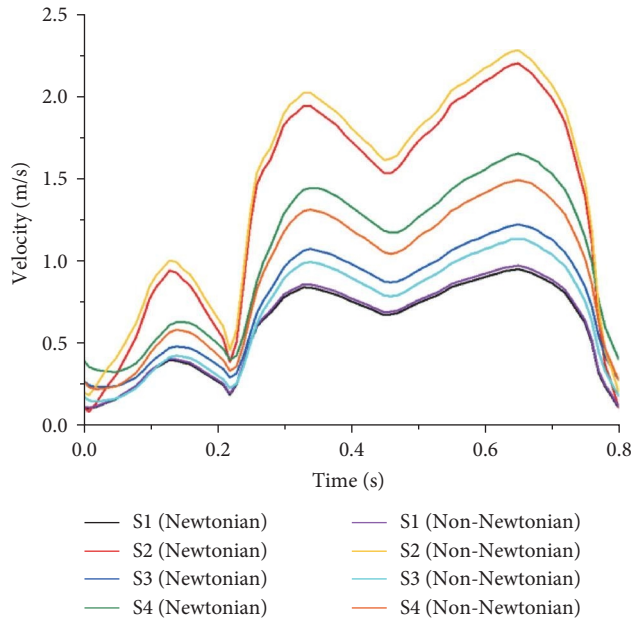

Figure 8: Maximum velocities on normal branches.

that the pressure values of non-Newtonian fluid are higher than those of Newtonian fluid. The pressure curves at both ends of the stenosis are shown in Figure 7. The pressure difference between section S5 (non-Newtonian) and S5 (Newtonian) is high. However, the pressure difference between section S6 (non-Newtonian) and S6 (Newtonian) may be almost ignored.

3.3. Maximum Velocities. As shown in Figure 8, the velocity distribution trends of sections S1, S2, S3, and S4 are the same as that of the inlet velocity. The velocities of section S1 (whether Newtonian or non-Newtonian) are lower than the inlet velocity, and the peak velocities of other sections are higher than the inlet peak velocity. Section S2 (whether Newtonian or non-Newtonian) is close to one of the outlets,

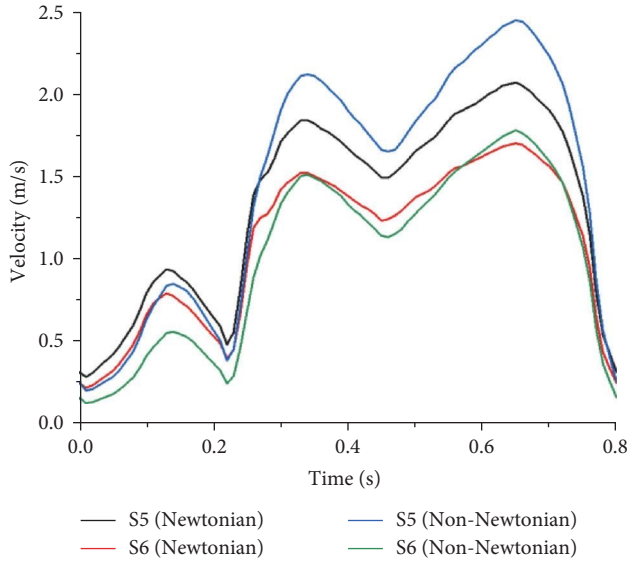

Figure 9: Maximum velocities at both ends of the stenosis.

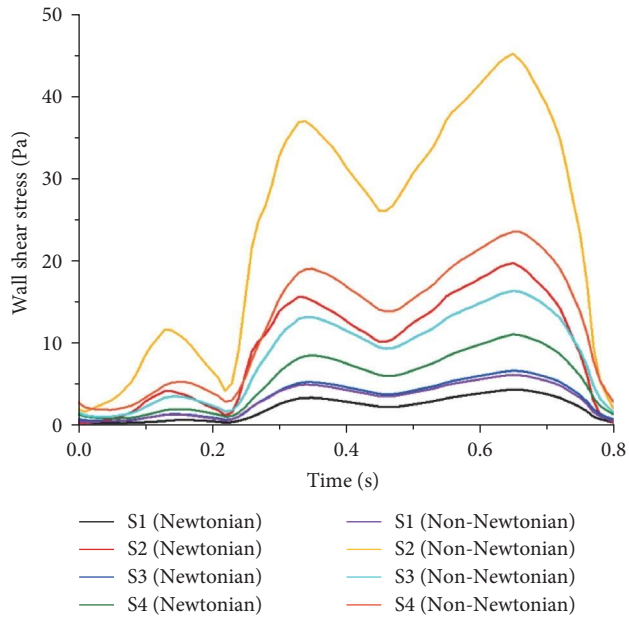

Figure 10: Maximum wall shear stresses on normal branches.

and the velocities reach the maximum, with the peak velocities of 2.15 and 2.25 m/s, respectively. Regardless of Newtonian or non-Newtonian fluids, the peak velocity of section S4 is higher than that of section S3. As shown in Figure 9, compared with the inlet velocity, the flow velocity at both ends of the stenosis is high. The peak velocity of section S5 (non-Newtonian) is nearly 2.5 m/s, and that of section S5 (Newtonian) is about 2 m/s. During systole, it can be seen that the peak velocities of section S6 (Newtonian) and S6 (non-Newtonian) are equal.

3.4. Maximum Wall Shear Stresses. As shown in Figure 10, the wall shear stresses of section S1 (whether Newtonian or non-Newtonian) are the lowest, and the peak value of section S1 (non-Newtonian) is about 5 Pa, which is not different from

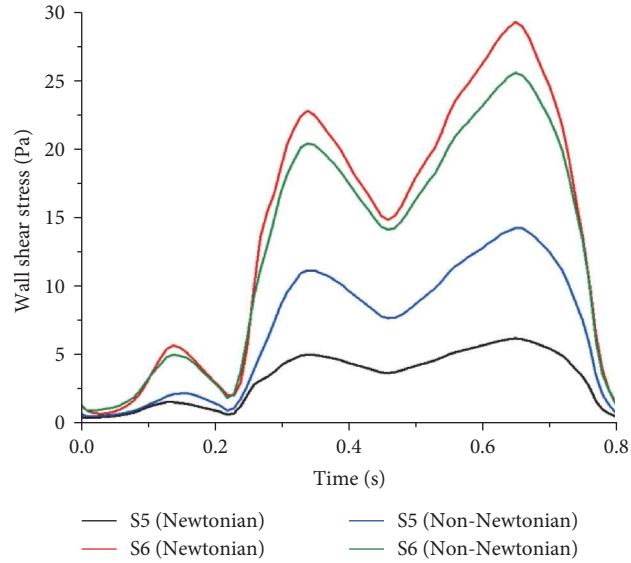

Figure 11: Maximum wall shear stresses at both ends of the stenosis.

that of section S3 (Newtonian). It is obvious that the peak wall shear stress of section S2 (non-Newtonian) is about 45 Pa, and the peak value of section S2 (Newtonian) is about 20 Pa. The wall shear stress curves of sections S3 and S4 with the two models are located in the middle of the curves of all sections. Figure 11 shows that the wall shear stress at the distal end is higher than that at the proximal end of the stenosis, and the peak values of section S6 (whether Newtonian or non-Newtonian) are above 20 Pa. The fluctuation range of the wall shear stress of section S5 (Newtonian) is higher than that of section S5 (non-Newtonian).

4. Discussion

According to the diagnostic report, it is clear that the local segment of the patient's right pulmonary artery is severely blocked; therefore, the hemodynamics in the artery must be affected by the stenosis. By comparing with previous studies, the change trend of hemodynamics in the nonstenosis region is in good agreement [28–30]. The influence factors of QPPR play an important role in clinical diagnosis and prediction. QPPR value shows that non-Newtonian fluid can better simulate the rheological properties of blood. When non-Newtonian fluid is used to simulate blood, the peak pressure at the proximal end of the stenosis is higher than that of Newtonian fluid, which indicates that the simulation effect of non-Newtonian fluid can more objectively reflect the severity of patient's blockage. In addition, there is a strong correlation between pulmonary vascular classification and the pressure ratio [3]. According to the classification standard, the simulation result of non-Newtonian fluid in this paper QPPR = 0.4367 is between pulmonary vascular classification levels 1 and 2, and interventional treatment is needed in clinic. Arterial stenosis limits the blood supply of tissues and significantly affects the development and formation of cardiovascular diseases. Due to arterial stenosis, the flow resistance of the right pulmonary artery will rise, resulting in a reduction in the distribution of arterial blood flow. There is a large pressure

drop in the pressure curves at both ends of the stenosis. The higher the pressure drop, the lower the QPPR. Due to blockage, the velocity of the proximal end of the stenosis is lower than that of the distal end. The unstable blood flow velocity will reduce effective blood flow and increase kinetic energy loss, and affect the physiological processes of vascular endothelial cells, such as promoting the proliferation and apoptosis of vascular endothelial cells and the uptake of lipids by endothelial cells, and strengthening the inflammatory response [31]. The change of blood flow velocity leads to the change of wall shear stress. High velocity leads to high wall shear stress. The range of normal arterial wall shear stress in human body is between 0.5 and 4 Pa [32]. According to the pressure results of simulation, it exceeds the normal physiological range of human body. These factors increase the risk of plaque rupture and have certain damage to human endothelial cells. According to the literature [33], high stress in the stenosis can promote megaphagocytes to produce matrix ferriprotease, cause matrix degradation, weaken the fibrous cap of plaque, and gradually evolve into thrombus and other diseases.

In recent years, with the development of computer technology and medical imaging, based on CT images of patients' pulmonary arteries, CFD is used to more accurately and intuitively simulate the blood flow state of real patients' pulmonary arteries and obtain QPPR and hemodynamic parameters, taking into account the impact of cardiac cycle on blood flow. However, there are still limitations in the current simulation. The real human blood vessels have the characteristics of viscoelasticity. The linear elastic wall model is used for the simplified simulation, and, thus, the result may deviate from the fact. In this study, only one stenosis pulmonary artery model is constructed, and the conditions will be continuously optimized in the future work. If the patient has multiple pulmonary artery blockages, multiple stenosis models will be constructed to simulate QPPR and hemodynamic changes.

5. Conclusion

Based on the real CT images of a patient with chronic thromboembolic pulmonary hypertension, the specific 3D model is constructed. Newtonian and non-Newtonian fluids are, respectively, used to simulate blood, and the effects of the two models on QPPR and hemodynamic characteristics are discussed using fluid–solid interaction. The results show that pressure and velocity decrease more and faster when blood flow enters into the stenosis region. There is a high wall shear stress in the stenosis downstream. The QPPR value of non-Newtonian fluid simulation is closer to the clinical measurement value. Therefore, the simulation effect of non-Newtonian fluid is more significant than that of Newtonian fluid. The analysis of this study confirms that the stenosis model simulated by a porous medium is of clinical significance, and non-Newtonian fluid simulation of blood flow is more convincing, which provides a quantitative analysis basis for clinical diagnosis and treatment.

Data Availability

The data used to support the findings of this study are included within the article.

Conflicts of Interest

The authors declare that they have no conflicts of interest.

Funding

The work is supported by the National Clinical Research Center for Cardiovascular Diseases, Fuwai Hospital, Chinese Academy of Medical Sciences (grant no. NCRC2020007), and CAMS Innovation Fund for Medical Sciences (2017-I2M-3-003) and the National High Level Hospital Clinical Research Funding (2022-GSP-QN-4).

References

[1] T. Saito, H. Kasai, T. Sugiura et al., "Effects of pulmonary endarterectomy on pulmonary hemodynamics in chronic thromboembolic pulmonary hypertension, evaluated by interventricular septum curvature," *Pulmonary Circulation*, vol. 10, no. 1, Article ID 2045894019897502, 2020.

[2] S. Jamieson and G. Victor Pretorius, "Chronic thromboembolic pulmonary hypertension," *Seminars in Interventional Radiology*, vol. 35, no. 2, pp. 136–142, 2018.

[3] T. Inami, M. Kataoka, N. Shimura et al., "Pulmonary Edema Predictive Scoring Index (PEPSI), a new index to predict risk of reperfusion pulmonary edema and improvement of hemodynamics in percutaneous transluminal pulmonary angioplasty," *JACC: Cardiovascular Interventions*, vol. 6, no. 7, pp. 725–736, 2013.

[4] K. S. Mekheimer, I. Shahzadi, S. Nadeem, A. M. A. Moawad, and A. Z. Zaher, "Reactivity of bifurcation angle and electroosmosis flow for hemodynamic flow through aortic bifurcation and stenotic wall with heat transfer," *Physica Scripta*, vol. 96, no. 1, Article ID 015216, 2020.

[5] A. M. Abdelwahab, K. S. Mekheimer, K. K. Ali, A. El-Kholy, and N. S. Sweed, "Numerical simulation of electroosmotic force on micropolar pulsatile bloodstream through aneurysm and stenosis of carotid," *Waves in Random and Complex Media*, pp. 1–32, 2021.

[6] S. Kamangar, I. A. Badruddin, K. Govindaraju et al., "Patient-specific 3D hemodynamics modelling of left coronary artery under hyperemic conditions," *Medical and Biological Engineering and Computing*, vol. 55, no. 8, pp. 1451–1461, 2017.

[7] M. Solecki, M. Kruk, M. Demkow et al., "What is the optimal anatomic location for coronary artery pressure measurement at CT-derived FFR?" *Journal of Cardiovascular Computed Tomography*, vol. 11, no. 5, pp. 397–403, 2017.

[8] B.-K. Koo, A. Erglis, J.-H. Doh et al., "Diagnosis of ischemia-causing coronary stenoses by noninvasive fractional flow reserve computed from coronary computed tomographic angiograms. Results from the prospective multicenter DISCOVER-FLOW (Diagnosis of Ischemia-Causing Stenoses Obtained Via Noninvasive Fractional Flow Reserve) study," *Journal of the American College of Cardiology*, vol. 58, no. 19, pp. 1989–1997, 2011.

[9] N. H. Pijls, J. A. van Son, R. L. Kirkeeide, B. De Bruyne, and K. L. Gould, "Experimental basis of determining maximum coronary, myocardial, and collateral blood flow by pressure measurements for assessing functional stenosis severity before and after percutaneous transluminal coronary angioplasty," *Circulation*, vol. 87, no. 4, pp. 1354–1367, 1993.

[10] T. Inami, M. Kataoka, N. Shimura et al., "Pressure-wire-guided percutaneous transluminal pulmonary angioplasty: a breakthrough in catheter-interventional therapy for chronic thromboembolic pulmonary hypertension," *JACC: Cardiovascular Interventions*, vol. 7, no. 11, pp. 1297–1306, 2014.

[11] J. K. Min, J. Leipsic, M. J. Pencina et al., "Diagnostic accuracy of fractional flow reserve from anatomic CT angiography," *JAMA*, vol. 308, no. 12, pp. 1237–1245, 2012.

[12] V. O. Kheyfets, J. Dunning, U. Truong, D. Ivy, K. Hunter, and R. Shandas, "A zero-dimensional model and protocol for simulating patient-specific pulmonary hemodynamics from limited clinical data," *Journal of Biomechanical Engineering*, vol. 138, no. 12, Article ID 121001, 2016.

[13] P. Ebrahimi, D. Youssef, G. Salve et al., "Evaluation of personalized right ventricle to pulmonary artery conduits using in silico design and computational analysis of flow," *JTCVS Open*, vol. 1, pp. 33–48, 2020.

[14] F. Kong, V. Kheyfets, E. Finol, and X.-C. Cai, "Simulation of unsteady blood flows in a patient-specific compliant pulmonary artery with a highly parallel monolithically coupled fluid–structure interaction algorithm," *International Journal for Numerical Methods in Biomedical Engineering*, vol. 35, no. 7, Article ID e3208, 2019.

[15] S. Sohrabi, J. Zheng, E. A. Finol, and Y. Liu, "Numerical simulation of particle transport and deposition in the pulmonary vasculature," *Journal of Biomechanical Engineering*, vol. 136, no. 12, Article ID 121010, 2014.

[16] A. M. Awad, K. S. Mekheimer, S. A. Elkilany, and A. Z. Zaher, "Leveraging elasticity of blood stenosis to detect the role of a non-Newtonian flow midst an arterial tube: Mazumdar and Keller models," *Chinese Journal of Physics*, vol. 77, pp. 2520–2540, 2022.

[17] S. F. Ramadan, K. S. Mekheimer, M. M. Bhatti, and A. M. A. Moawad, "Phan-Thien-Tanner nanofluid flow with gold nanoparticles through a stenotic electrokinetic aorta: a study on the cancer treatment," *Heat Transfer Research*, vol. 52, no. 16, pp. 87–99, 2021.

[18] L. Zhang, M. M. Bhatti, M. Marin, and K. S. Mekheimer, "Entropy analysis on the blood flow through anisotropically tapered arteries filled with magnetic zinc-oxide (ZnO) nanoparticles," *Entropy*, vol. 22, no. 10, Article ID 1070, 2020.

[19] C. Kumawat, B. K. Sharma, and K. S. Mekheimer, "Mathematical analysis of two-phase blood flow through a stenosed curved artery with hematocrit and temperature dependent viscosity," *Physica Scripta*, vol. 96, no. 12, Article ID 125277, 2021.

[20] N. Bessonov, A. Sequeira, S. Simakov, Y. Vassilevskii, and V. Volpert, "Methods of blood flow modelling," *Mathematical Modelling of Natural Phenomena*, vol. 11, no. 1, pp. 1–25, 2016.

[21] E. Doutel, S. I. S. Pinto, J. B. L. M. Campos, and J. M. Miranda, "Link between deviations from Murray's law and occurrence of low wall shear stress regions in the left coronary artery," *Journal of Theoretical Biology*, vol. 402, pp. 89–99, 2016.

[22] S. Mosbahi, E. Mickaily-Huber, D. Charbonnier et al., "Computational fluid dynamics of the right ventricular outflow tract and of the pulmonary artery: a bench model of flow dynamics," *Interactive CardioVascular and Thoracic Surgery*, vol. 19, no. 4, pp. 611–616, 2014.

[23] Y.-C. Fung, *Biomechanics: Mechanical Properties of Living Tissues*, Springer-Verlag, New York, 1993.

[24] C. A. Taylor and J. D. Humphrey, "Open problems in computational vascular biomechanics: hemodynamics and arterial wall mechanics," *Computer Methods in Applied Mechanics and Engineering*, vol. 198, no. 45–46, pp. 3514–3523, 2009.

[25] T. J. Pedley, *The Fluid Mechanics of Large Blood Vessels*, Cambridge University Press, London, 1980.

[26] Y. C. Fung and B. W. Zweifach, "Microcirculation: mechanics of blood flow in capillaries," *Annual Review of Fluid Mechanics*, vol. 3, pp. 189–210, 1971.

[27] D. Y. Leung and M. Leung, "Significance and assessment of coronary microvascular dysfunction," *Heart*, vol. 97, no. 7, pp. 587–595, 2011.

[28] M. Udupa, S. Shankar Narayan, and S. Saha, "A study of the blood flow using Newtonian and non-Newtonian approach in a stenosed artery," in *Proceedings of International Conference on Trends in Computational and Cognitive Engineering*, pp. 257–269, Springer, Singapore, 2021.

[29] B. D. Plourde, L. J. Vallez, B. Sun, B. B. Nelson-Cheeseman, J. P. Abraham, and C. S. Staniloae, "Alterations of blood flow through arteries following atherectomy and the impact on pressure variation and velocity," *Cardiovascular Engineering and Technology*, vol. 7, no. 3, pp. 280–289, 2016.

[30] Y. H. Qiao, Y. J. Zeng, Y. Ding, J. R. Fan, K. Luo, and T. Zhu, "Numerical simulation of two-phase non-Newtonian blood flow with fluid-structure interaction in aortic dissection," *Computer Methods in Biomechanics and Biomedical Engineering*, vol. 22, no. 6, pp. 620–630, 2019.

[31] C. L. Feldman, O. J. Ilegbusi, Z. Hu, R. Nesto, S. Waxman, and P. H. Stone, "Determination of in vivo velocity and endothelial shear stress patterns with phasic flow in human coronary arteries: a methodology to predict progression of coronary atherosclerosis," *American Heart Journal*, vol. 143, no. 6, pp. 931–939, 2002.

[32] W. V. Potters, H. A. Marquering, E. VanBavel, and A. J. Nederveen, "Measuring wall shear stress using velocity-encoded MRI," *Current Cardiovascular Imaging Reports*, vol. 7, Article ID 9257, 2014.

[33] A. K. Chaniotis, L. Kaiktsis, D. Katritsis, E. Efstathopoulos, I. Pantos, and V. Marmarellis, "Computational study of pulsatile blood flow in prototype vessel geometries of coronary segments," *Physica Medica: European Journal of Medical Physics*, vol. 26, no. 3, pp. 140–156, 2010.